Supplementary Information for
Velocity Saturation in Digital Microfluidics

Ian Swyer,[a] Ryan Fobel,[b] and Aaron R. Wheeler[a,b,c,‡]

[a] Department of Chemistry, University of Toronto, 80 St George St., Toronto, ON, M5S 3H6, Canada

[f] Donnelly Centre for Cellular and Biomolecular Research, University of Toronto, 160 College St, Toronto, ON, M5S 3E1, Canada

[g] Institute for Biomaterials and Biomedical Engineering, University of Toronto, 164 College St, Toronto, ON, M5S 3G9, Canada

‡ Corresponding author

1 Dimensionless number analysis

The quasi-static assumption made in the main text can be justified if inertial forces are small relative to surface tension, a relationship quantified by the non-dimensional Weber number,

$$W_{\mathrm{e}} = \frac{\text{inertial forces}}{\text{surface tension forces}} = \frac{\rho L}{\gamma}(\frac{dx}{dt})^2$$

where ρ is liquid density, L is the characteristic length (i.e., the electrode pitch in a DMF device), dx/dt is the droplet velocity, and γ is surface tension. The highest Weber number that we expect for the experiments described in the main text is for a droplet of water moving at 70 mm/s on 2.25 mm x 5 mm electrodes, which has $W_e \sim 0.15$. Even this "worst-case" scenario is well below the critical Weber number at which droplets become unstable and break up, $W_{e,critical} \sim 10$.[1,3]

The derivation in the main text also assumes that inertia is insignificant relative to viscous forces, a ratio described by the non-dimensional Reynolds number,

$$R_{\mathrm{e}} = \frac{\text{inertial forces}}{\text{viscous forces}} = \frac{\rho L}{\mu}(\frac{dx}{dt})$$

where μ is the dynamic viscosity of the liquid. For our experimental system, the highest expected Reynolds number is $R_e \sim 160$ for a droplet of water moving at 70 mm/s on 2.25 mm x 5 mm electrodes. This is well below the critical Reynolds number at which Poiseuille flow between parallel plates becomes turbulent, $R_{e,critical} \sim 5000$.[2]

Finally, the analysis in the main text assumes that surface tension dominates viscous forces, a property addressed by the non-dimensional capillary number.

$$C_{\mathrm{a}} = \frac{\text{viscous forces}}{\text{surface tension forces}} = \frac{\mu}{\gamma}(\frac{dx}{dt})$$

For a droplet of water moving at up to 70 mm/s, $C_a < 10^{-3}$, suggesting that surface tension is the dominant force that determines the shape of the droplet once the flow is fully developed.

2 Electrical and Fluidic Time Constants

The longest duration for charging/de-charging of the electrical circuit in this system is the case in which a droplet completely covers an actuated electrode, measured to be approx. 50 pF. (Note that when the electrode is covered by air, the capacitance is approximately two orders of magnitude lower.) Further, the traces leading to the actuation electrodes have a resistance of approximately 500 Ω, such that the RC time constant for the system is given below.

$$\tau = RC = (500\ \Omega)(5 \times 10^{-11}\ \mathrm{F}) = 25\ \mathrm{ns}$$

The shortest duration for fluidic acceleration/deceleration in the droplets evaluated in this work is for aqueous solutions containing pluronics. The time constant in this case determined by dividing droplet mass ($m = 0.0028$ g) by the velocity-sensitive dissipation coefficient $k_d = 0.0051$ kg s^{-1}.

$$\frac{m}{k_\mathrm{d}} = \frac{0.0028 \text{ g}}{5.1 \text{ g s}^{-1}} = 0.00055 \text{ s} = 550 \ \mu\text{s}$$

Thus, for the work presented here, the timescale for capacitive charging/discharging is more than 10^4 times faster than that of droplet acceleration/deceleration. Given this relationship, it is appropriate to treat the system's electrical behaviour as being instantaneous from the point of view of the droplet dynamics.

3 Comparison of Capacitance and Optical Measurements of Position

As a more detailed examination of the relationship between capacitance-derived and optical-derived measurements, 2.8 μL droplets of an aqueous solution of 0.1 mg/mL L64 and 0.1 M NaCl were driven from an origin to a destination electrode by applying width-normalized driving forces of 12 mN/m at a frequency of 10 kHz, during which videos were captured with a Pixel 3 phone camera through the 10x eye-piece of a dissection microscope equipped with a 4x zoom using a ring illumination light source.

Since the sampling rate of the camera and the capacitance measurement do not match, we limit the analysis to capacitance data that are collected at integer multiples of the frame rate (240 fps) of the camera $\pm$ 0.0005 s. That is, capacitance data were retrieved and analyzed when the following relation holds, and then were converted to position as described in the main text.

$$t_\mathrm{capacitance} = \frac{n}{240} \pm 0.0005 \text{ s where } n = 1, 2, 3...$$

Capacitance-derived distances collected as described above were compared to measurements of position from the camera, which were estimated by dividing the length of the destination electrode into ten 0.5 mm-long segments. The position of each droplet was marked as the position at the center of the droplet that penetrated the furthest onto the actuated electrode. Note that the capacitance measurements assume a rectangular droplet and cannot account for the curvature at the leading edge of the droplet. This bias is not relevant when measuring droplet velocities, but for this analysis, it was compensated by using the frame collected at $t = 0.675$ s to determine a constant that accounts for droplet curvature (0.092mm), and adding that value to all of the capacitance-derived data. After this calibration, capacitance-derived data were plotted as a function of time [figure S1 (a)], and compared to corresponding frames from the camera [figure S1 (b)]. As shown, the two sets of measurements are close, with the standard deviation describing the variance between the two measurements of 0.025 mm ($n = 5$).

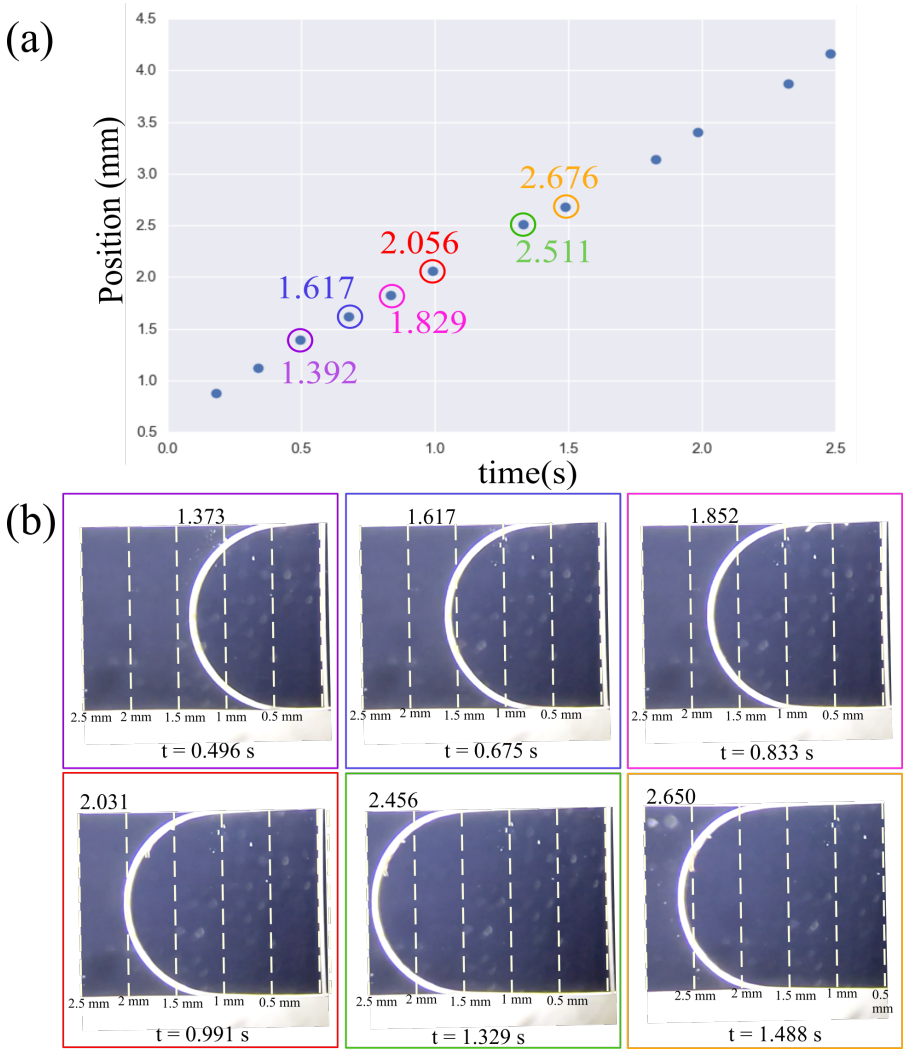

Figure S1: Comparison of capacitance and visual measurements of droplet position. (a) Capacitance-derived droplet position as a function of time (solid blue circles) for a 0.1 mg/mL L64 + 0.1 M NaCl solution moving on to an actuated electrode. The precise capacitance-derived position measurements are indicated for t = 0.496 (violet), 0.675 (blue), 0.833 (pink), 0.991 (red), 1.329 (green), and 1.488 s (yellow). (b) Camera frames with rectangular outlines color-coded to correspond with the capacitance-derived position data in (a). Each frame is divided into 0.5 mm-long sections (white dashed lines). The camera-derived droplet position is recorded at the top of each frame.

4 Replicate Force-Velocity Curves

Force-velocity plots were collected as described in the main text for aqueous 0.1 mg/mL L64, aqueous 0.01 mg/mL L64, neat dimethyl formamide, aqueous 0.01 mg/mL L64 with 0.1 M NaCl, and aqueous 0.1 mg/mL L64 with 0.1 M NaCl. The raw data (as well as the individual extracted saturation forces and their averages and standard deviations) are found in Figures S2, S3, S4, S5, and S6 respectively.

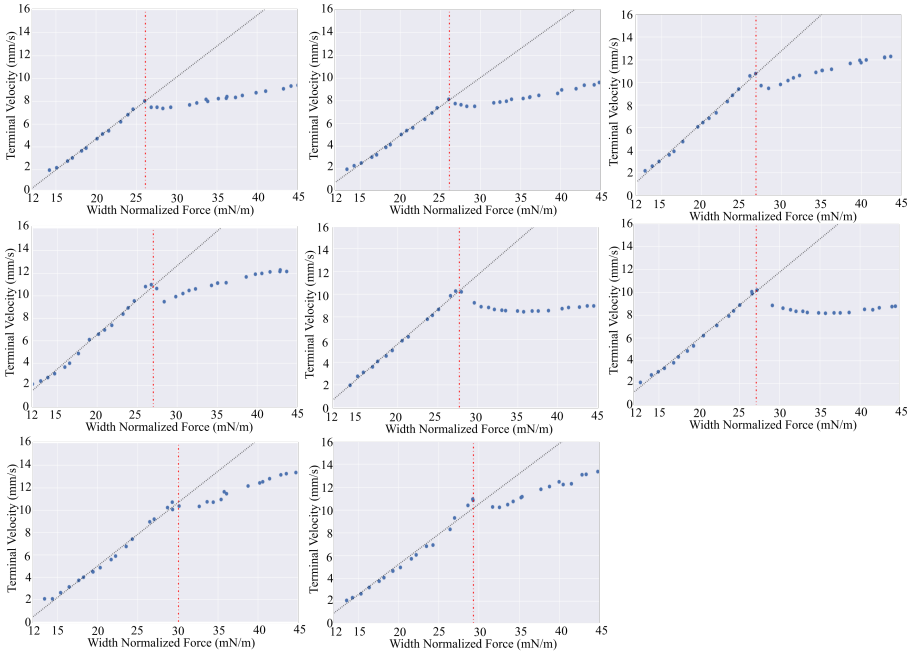

Saturation Force (mN/m)								Average (mN/m)	STD (mN/m)
26.1	26.1	26.8	27	27.7	27.1	30.1	29.3	27.5	1.5

Figure S2: Force-velocity plot replicates for aqueous 0.1 mg/mL L64 solutions. In each plot, the blue circles are the capacitance-derived velocity data, the dotted black line represents the linear regression for data below saturation, and the dotted red line represents the saturation force. The table below the plots summarizes the saturation forces for each replicate as well as the average saturation force and standard deviation.

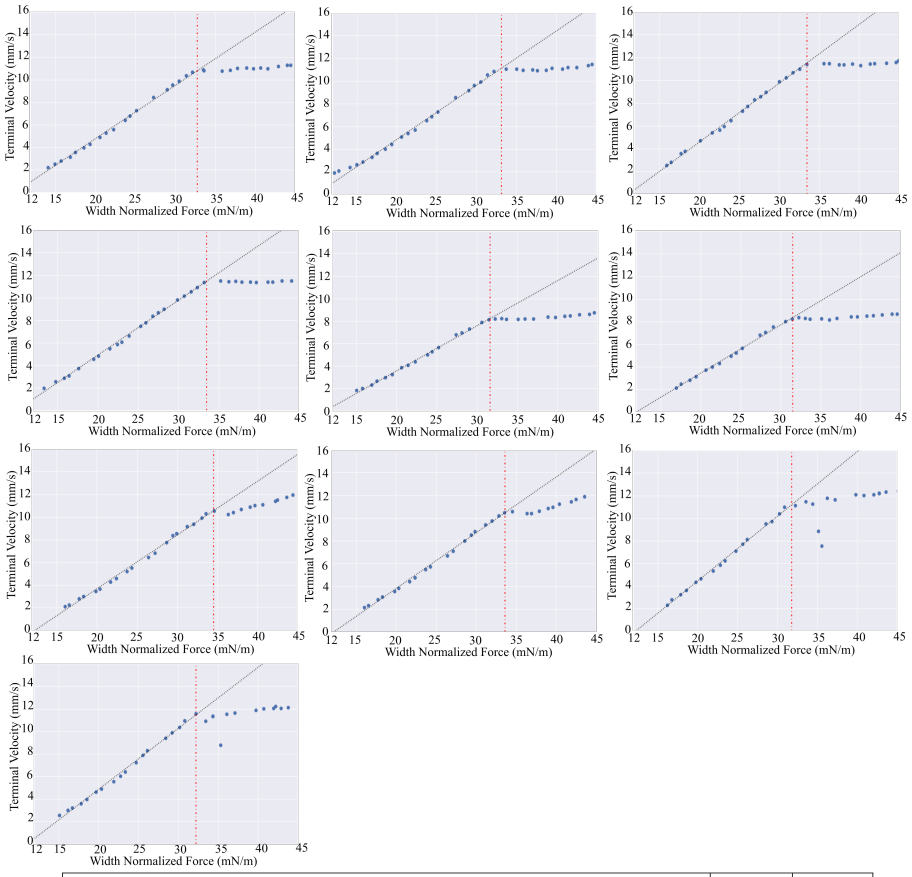

Saturation Force (mN/m)										Average (mN/m)	STD (mN/m)
32.7	33.1	33.5	33.5	31.6	31.5	34.5	33.6	31.8	32.2	32.8	1.0

Figure S3: Force-velocity plot replicates for aqueous 0.01 mg/mL L64 solutions. In each plot, the blue circles are the capacitance-derived velocity data, the dotted black line represents the linear regression for data below saturation, and the dotted red line represents the saturation force. The table below the plots summarizes the saturation forces for each replicate as well as the average saturation force and standard deviation.

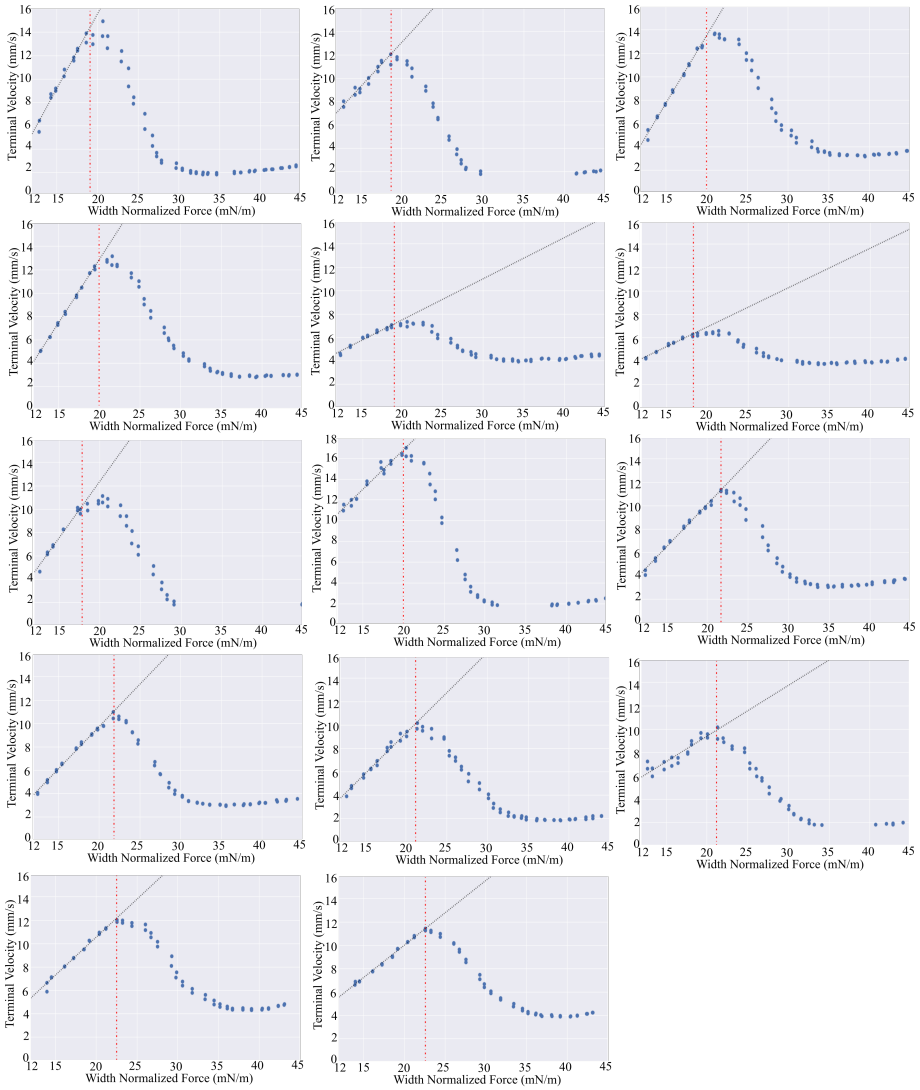

Saturation Force (mN/m)														Average (mN/m)	STD (mN/m)
19.1	18.7	20	20	19.1	18.3	17.8	20	21.7	21.8	21.2	21.2	22.5	22.6	20.3	1.6

Figure S4: Force-velocity plot replicates for neat dimethylformamide. In each plot, the blue circles are the capacitance-derived velocity data, the dotted black line represents the linear regression for data below saturation, and the dotted red line represents the saturation force. The table below the plots summarizes the saturation forces for each replicate as well as the average saturation force and standard deviation.

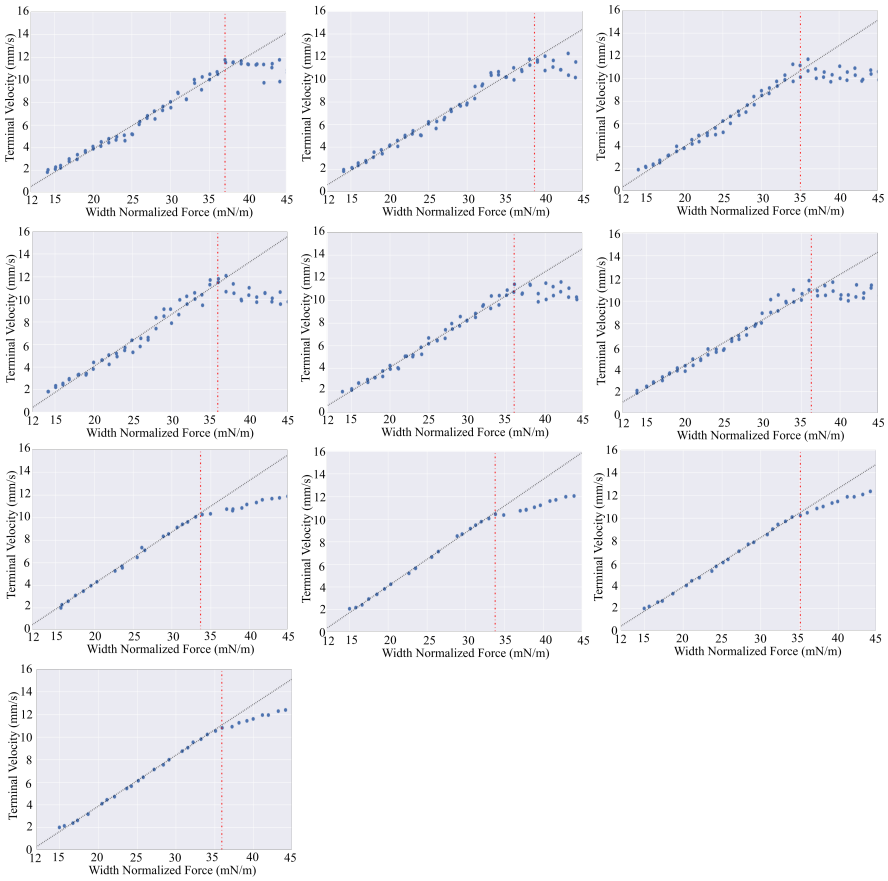

Saturation Forces (mN/m)										Average (mN/m)	STD (mN/m)
37	38.7	35	36.3	36	36.3	33.7	33.8	35.1	35.9	35.8	1.5

Figure S5: Force-velocity plot replicates for aqueous 0.01 mg/mL L64 + 0.1 M NaCl solutions. In each plot, the blue circles are the capacitance-derived velocity data, the dotted black line represents the linear regression for data below saturation, and the dotted red line represents the saturation force. The table below the plots summarizes the saturation forces for each replicate as well as the average saturation force and standard deviation.

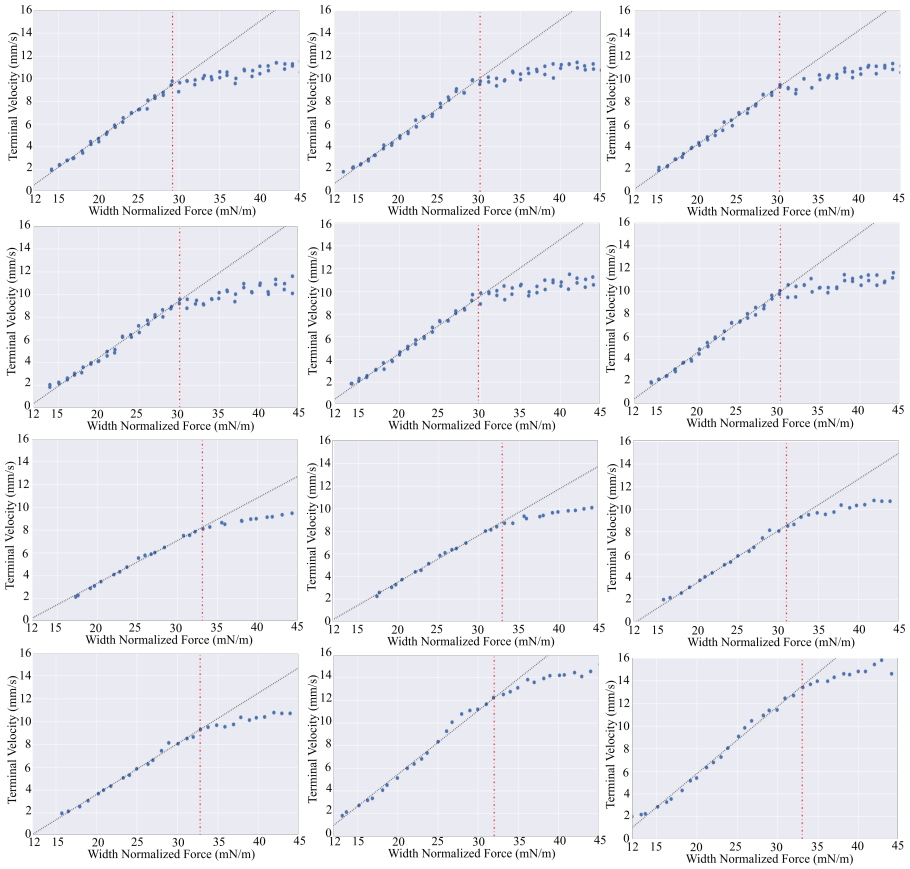

Saturation Forces(mN/m)												Average (mN/m)	STD (mN/m)
29.2	30	30	30.1	29.8	29.9	33.6	31.7	30.1	32.8	33	33	31.1	1.6

Figure S6: Force-velocity plot replicates for aqueous 0.1 mg/mL L64 + 0.1 M NaCl solutions. In each plot, the blue circles are the capacitance-derived velocity data, the dotted black line represents the linear regression for data below saturation, and the dotted red line represents the saturation force. The table below the plots summarizes the saturation forces for each replicate as well as the average saturation force and standard deviation.

References

[1] JO Hinze. Critical speeds and sizes of liquid globules. *Flow, Turbulence and Combustion*, 1(1):273, 1949.

[2] CC Kin. *The theory of hydrodynamic stability.* Cambridge University Press, Cambridge, 1955.

[3] A Wierzba. Deformation and breakup of liquid drops in a gas stream at nearly critical weber numbers. *Experiments in Fluids*, 9(1-2):59–64, 1990.